Genome Biology

RESEARCH

Open Access

Functional characterization of transporter genes in rice node at single-cell resolution through multi-omics technologies

Hu Li[1†], Huiling Jin[1†], Min Ning[1,2†], Fenglin Deng[3,4], Wenyi Chen[1], Ou Yang[1], Jianhui Cheng[3], Xiaoping Lian[1], Lin Shao[1], Shilai Zhang[1], Naoki Yamaji[2], Fengyi Hu[1], Jian Feng Ma[2] and Gui Jie Lei[1*]

[†]Hu Li, Huiling Jin and Min Ning contributed equally to this work.

*Correspondence: Leigj@ynu.edu.cn

[1] State Key Laboratory for Vegetation Structure, Key Laboratory of Biology and Germplasm Innovation of Perennial Rice, Center of Innovation for Perennial Rice Technology in Yunnan, Key Laboratory of Crop Quality Improvement of Yunnan Higher Education Institutes, New Cornerstone Science Laboratory, School of Agriculture, Yunnan University, Kunming 650500, China
[2] Institute of Plant Science and Resources, Okayama University, Kurashiki 710-0046, Japan
[3] MARA Key Laboratory of Sustainable Crop Production in the Middle Reaches of the Yangtze River, College of Agriculture, Yangtze University, Jingzhou 434025, China
[4] Hubei Hongshan Laboratory, Wuhan 430070, China

Abstract

Background: The rice node is a critical hub for the distribution of mineral nutrients, mediated by transporters. Manganese (Mn) is an essential micronutrient for plant growth. However, the precise cell types and the cell-type-enriched transporter genes in rice node, and the molecular mechanisms underlying the translocation and distribution of Mn in rice remain poorly understood.

Results: We characterize 11 distinct cell types using multiple cluster-enriched genes in rice node I through single-nucleus RNA sequencing (snRNA-seq), systematically profile the expression patterns of putative 1,144 transporter genes within 11 cell types, and identify six candidate transporter genes linked to the tissue-specific deposition of six elements through combining spatial ionomics in node, respectively. Furthermore, we functionally characterize *OsMTP7* that is highly expressed in phloem cells in node, as well as in root stele cells and anther. OsMTP7 is localized to plasma membrane in rice and shows efflux activity for Mn. *OsMTP7* knockout inhibites Mn uptake and xylem-mediated Mn translocation in root and Mn distribution in node, leading to decreased Mn concentration in various organs and root xylem sap, resulting in reduced biomass and yield. We reveal that *OsMTP7* knockout alters expression of genes for multiple biological processes in spikelets using bulk RNA-seq, resulting in increased oxidative stress in anther and low fertility.

Conclusions: Our study reveals the precise cell types and the cell-type-enriched transporter genes in node, identifies candidate transporters for elements deposition in node, and demonstrates a novel and critical Mn efflux transporter mediating Mn uptake, translocation and distribution for improving growth and yield in rice.

Keywords: Rice, Node, snRNA-seq, Transporter, Ionomics, Manganese, Multi omics

Background

Mineral elements are absorbed by roots and then translocated to shoots via xylem, driven by root pressure and leaf transpiration. Theoretically, few elements will be distributed to the developing organs, such as the newest leaf and panicle, due to their small surface area and low transpiration rate. However, these developing organs usually require and contain abundant mineral nutrients for active growth [1, 2]. In the past decade, the node, particularly the uppermost node/node I directly linked to the flag leaf and panicle, has been identified as the critical hub for the preferential and efficient distribution of mineral nutrients to developing organs in plants, including barley, maize, Arabidopsis, and especially rice [3–7].

The node is a crucial junction organ connecting internodes, leaves, and axillary buds/tillers. Rice typically has 4–5 elongated nodes on a main tiller at the reproductive stage although 13–18 nodes in total [2, 8]. Each rice node contains three primary types of axial vascular bundles (VBs), including enlarged VB (EVB), transit VB (TVB), and diffuse VB (DVB) [2, 3]. The vascular connectivity follows a specific pattern. EVB in node n (EVB_n) directly links TVB of the lower node (TVB_{n-1}) and $leaf_n$. TVB_n directly connects DVB_{n-1} and EVB of the upper node (EVB_{n+1}). DVB_n connects to TVB_{n+1}. Additionally, the horizontal nodal vascular anastomosis (NVA) establishes a direct link between three VBs at the basal part of each node. Crucially, the inter-vascular transfer from EVB to DVB within each node facilitates the preferential and efficient distribution of nutrients to developing organs. The parenchyma cell bridge (PCB), located between EVB and DVB, is a key tissue enabling this inter-vascular nutrient movement. VBs and NVA comprise both xylem and phloem regions, while PCB is distinguished by densely packed plasmodesmata [2, 3]. Beyond these components, rice node contains other complex and highly organized tissues [2, 3, 8], while the precise cellular composition remains incompletely characterized.

The inter-vascular transfer in node is mediated by various transporters. To date, only some of transporters involved in the three key steps of the inter-vascular transfer have been characterized in rice. In step one, OsLsi6 for silicon (Si) [9], OsZIP3 for zinc (Zn) [10], and OsOPT7 for iron (Fe) are specifically localized in EVB xylem [11], OsPHO1;2 for phosphorus (P) is localized in xylem of EVB primarily and DVB partially [12], and OsHMA5 for copper (Cu) is primarily localized in DVB xylem [13], which mediate ion transport from xylem to PCB or phloem. In step two, OsLsi2 and OsLsi3 for Si are mainly localized in bundle sheath cells and PCB [9], respectively, and OsVMT for 2'-deoxymugineic acid is localized in PCB [14, 15], which mediate ion transport from EVB xylem to PCB or from PCB to DVB. In step three, OsPHO1;1 for P is primarily localized in DVB phloem [12, 16], and OsZIP4 and OsHMA2 for Zn are localized in phloem of DVB and EVB [17, 18], which mediate ion transport into phloem. However, the cell-type-specific expression patterns of other transporter genes within rice node remain poorly understood.

Manganese (Mn) is an essential micronutrient for plant growth and development. Mn serves as a cofactor or component in over 30 enzymes, playing an indispensable role in key biological processes such as photosynthesis, respiration, reactive oxygen species (ROS) scavenging, and hormone signaling [19, 20]. Plants require only trace amounts of Mn, but Mn^{2+} concentration in soil solutions can vary widely, from sub-micromolar to

millimolar levels, depending on soil conditions, posing risks of both deficiency and toxicity [19, 20]. To adapt to these fluctuations, plants have evolved complex Mn homeostasis systems regulated by diverse transporters. For example, rice OsNRAMP5 and OsMTP9 with polarity localization, as well as OsNRAMP1, play key roles in Mn uptake in root [21–23]. OsMTP8.1 and OsMTP8.2 regulate intracellular Mn storage via transporting Mn into vacuole [24, 25]. The Golgi-localized Mn transporters OsPML3 and OsMTP11 also contribute to Mn homeostasis [26, 27]. Additionally, OsMTP9, OsYSL2, OsYSL6, OsNRAMP3, and OsNRAMP5 are involved in translocation or distribution of Mn in root, leaf or node [22, 28–31]. However, the molecular mechanisms underlying Mn efflux either in root stele cells for translocation or in node for distribution are unknown.

Single-cell RNA sequencing (scRNA-seq) is a powerful technology that has revolutionized the study of plant biology by enabling the exploration of plant-specific cell types, cellular developmental trajectories, stress responses, and the identification of key genes involved in various biological processes [32, 33]. This approach relies on either protoplast isolation or single nuclei capture, both of which yield comparable transcriptomic information [34]. Single-nucleus RNA sequencing (snRNA-seq) has been particularly advantageous for analyzing organs and tissues where protoplast isolation is challenging [33]. In rice, scRNA-seq has been successfully applied to tissues such as plumule, root, culm, leaf, shoot apex, tiller bud, panicle, and spikelet or seed [34–39], except for node. Here, we first characterized 11 distinct cell types in rice node I at the single cell resolution using snRNA-seq, systematically profiled the expression patterns of various transporter genes across these cell types, and identified candidate transporter genes for the varied deposition patterns of elements. Notably, we functionally validated the critical role of OsMTP7 in maintaining Mn homeostasis and improving grain yield in rice.

Results

SnRNA-seq analysis of rice node I

To dissect the cellular heterogeneity of rice node I at single-cell resolution, nuclei were isolated from node I samples at three developmental stages: booting (RNA3), flowering (RNA2), and filling (RNA1) stages (Fig. 1A, Additional file 1: Fig. S1A), respectively. SnRNA-seq was performed using the 10 × Genomics Chromium platform. Raw reads were mapped to the T2T reference genome of Nipponbare [40], yielding a gene expression matrix encompassing 23,143 genes across 46,669 high-quality nuclei (Additional file 2: Table S1). Stage-specific counts included 10,064 (booting stage), 20,533 (flowering stage), and 16,072 (filling stage) nuclei (Additional file 1: Fig. S1B), with median gene counts of 1,125, 1,254, and 1,143, and median UMI counts of 1,716, 1,871, and 1,764 per nucleus, respectively (Additional file 2: Table S1). For downstream comparative analyses, nuclei from all three stages were first integrated to correct for batch effects and generate a unified dataset in a shared high-dimensional expression space. The integrated data were then subjected to linear dimensionality reduction using principal component analysis (PCA), retaining the top 30 principal components and performing graph-based clustering at a resolution of 0.2. The resulting clusters were visualized using UMAP and t-SNE, which consistently revealed 11 distinct cell clusters conserved across developmental stages (Fig. 1B, Additional file 1: Fig. S2). On the other hand, the ratios of 11 cell clusters in three samples of node I were similar (Additional

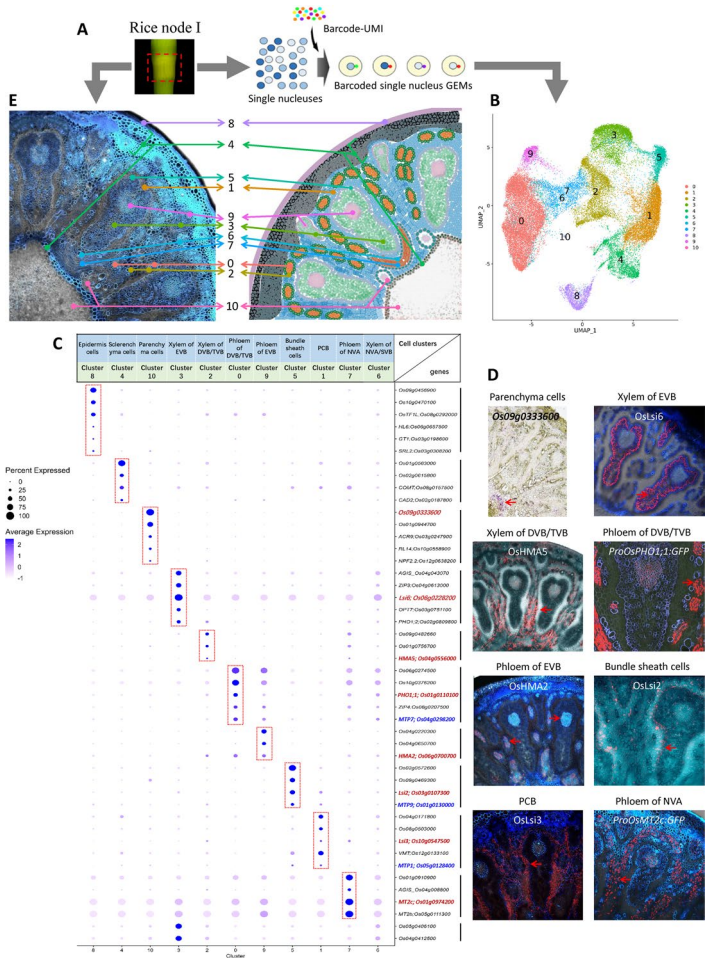

Fig. 1 SnRNA-seq analysis and cell types annotation of rice node I. **A** Overview of snRNA-seq workflow using rice node I. Plants were grown in a ½ Kimura B solution until reproductive stage, and then nuclei were isolated from each sample containing over 20 node I samples. SnRNA-seq libraries were generated using the 10 × Genomics platform, followed by high-throughput sequencing. **B** UMAP visualization of 11 cell clusters from 46,669 cells in three samples of rice node I from the booting stage, flowering stage, and filling stage. Each dot denotes a single cell. Colors denote corresponding cell clusters. **C** Expression patterns of representative marker or enriched genes for 11 cell types. The two most enriched genes and several confirmed or reported genes in each cell cluster were shown. Dot diameter represents the proportion of a given gene expressed in one specific cell cluster, and color represents their relative expression levels in these cell clusters. Enlarged vascular bundles, EVB; diffuse vascular bundles, DVB; transit vascular bundles, TVB; parenchyma cell bridge, PCB; nodal vascular anastomosis, NVA; small vascular bundles, SVB. **D** Tissue localization of eight marker or enriched genes in node I. RNA in situ hybridization for *Os09g0333600*. Immunostaining was performed using an antibody of OsLsi6, OsHMA5, OsHMA2, OsLsi2 or OsLsi3 in WT plants, or GFP antibody in transgenic lines carrying *ProOsPHO1;1:GFP* or *ProOsMT2c:GFP*. The purple or red color shows the signal from RNA in situ hybridization or an antibody, respectively. The blue/cyan color shows signal from cell wall autofluorescence. **E** Schematic illustration of various tissues in rice node I based on the anatomical morphology analysis and cell types annotation of snRNA-seq

file 1: Fig. S1B), and the spearman correlation analysis of pseudo-bulked expression profiles from each cell cluster showed that homologous clusters from different samples were highly correlated (Additional file 1: Fig. S1C), except for cluster 10. These results indicated that the identified differentially expressed genes and cluster identities are reproducible across growth stages, and genes likely showed similar expression patterns in the three growth stages.

Annotation of cell types in rice node I

To assign cell identities, 1,837 cluster-enriched genes were identified through differential expression analysis across clusters (Additional file 2: Table S2), and an expression heatmap of the selected top enriched genes was generated for each cluster (Additional file 1: Fig. S3). The expression patterns of the two most enriched genes and several confirmed or reported genes in each cell cluster were shown for 11 cell types annotation (Fig. 1C, Additional file 1: Fig. S4). Specifically, (1) RNA in situ hybridization of *Os09g0333600*, the top marker gene of Cluster 10, showed high expression in parenchyma cells (Fig. 1D). Furthermore, *OsACR9* and *OsRL14*, enriched in Cluster 10 (Additional file 2: Table S2), and *OsNPF2.2*, showing high expression in parenchyma or mesophyll cells [41–43], indicated Cluster 10 as parenchymal (Fig. 1C, E, Additional file 1: Fig. S4). (2) Cluster 3 was characterized by EVB xylem enriched genes, *OsZIP3*, *OsLsi6*, *OsOPT7*, and *OsPHO1;2* [9–12]. OsLsi6 localization was confirmed through immunostaining using its antibody (Fig. 1D), indicating Cluster 3 as EVB xylem cells (Fig. 1C, E, Additional file 1: Fig. S4). (3) *OsHMA5*, predominantly expressed in DVB xylem confirmed by immunostaining (Fig. 1D) [13], showed a similar expression profile to the top two markers of Cluster 2, suggesting that Cluster 2 represents DVB/TVB xylem cells (Fig. 1C, E, Additional file 1: Fig. S4). (4) Cluster 0 was characterized by *OsPHO1;1* that primarily expressed in DVB phloem, confirmed by immunostaining using GFP antibody in transgenic lines carrying *ProOsPHO1;1:GFP* (Fig. 1D) [12]. It indicated that Cluster 0 corresponds to DVB/TVB phloem cells (Fig. 1C, E, Additional file 1: Fig. S4). (5) *OsZIP4* and *OsHMA2*, enriched in both Clusters 0 and 9 (Additional file 2: Table S2), were highly expressed in DVB and EVB phloem [17, 18]. The tissue localization of OsHMA2 was confirmed by immunostaining (Fig. 1D), implying Cluster 9 as EVB phloem cells (Fig. 1C, E, Additional file 1: Fig. S4). (6) Cluster 5 was defined by *OsLsi2* with high expression in bundle sheath cells [9, 15], which was confirmed using immunostaining (Fig. 1D), indicating its identity as bundle sheath cells (Fig. 1C, E, Additional file 1: Fig. S4). (7) *OsLsi3* and *OsVMT* with high expression in PCB [9, 14], which was confirmed by immunostaining using OsLsi3 antibody (Fig. 1D), showed expression patterns similar to the top markers of Cluster 1, suggesting that Cluster 1 represents PCB (Fig. 1C, E, Additional file 1: Fig. S4).

Besides, (8) *OsMT2c* and *OsMT2b*, previously reported to be highly expressed in DVB and EVB phloem [44], were enriched in both Cluster 9 (EVB phloem) and Cluster 7 (Additional file 2: Table S2), with higher expression in Cluster 7 (Fig. 1C, Additional file 1: Fig. S4). Further study using *ProOsMT2c:GFP* transgenic line indicated that GFP expression was higher in NVA phloem than in phloem of DVB and EVB (Figs. 1D, 2E, Additional file 1: Fig. S5), suggesting cluster 7 as NVA phloem cells (Fig. 1C, E, Additional file 1: Fig. S4). (9) *Os05g0406100* and *Os04g0412500* were classified as the enriched genes of cluster 6, but primarily expressed in Cluster 3/EVB xylem (Fig. 1C, E, Additional file 1: Fig. S4). Notably, Cluster 6 was closely related to Cluster 7 (Fig. 1B), and the enriched genes from Cluster 3/EVB xylem also exhibited high expression in Cluster 6 (Additional file 1: Fig. S4). These findings suggest that Cluster 6 might represent xylem of NVA or small VBs (SVB) (Fig. 1C, E, Additional file 1: Fig. S4), while further investigation is required to confirm.

Additionally, (10) *OsTF1L* [45], *OsGT1* [46] and *OsSRL2* [47], mainly expressed in epidermal cells as confirmed by in situ hybridization previously, and *OsHL6*, regulating

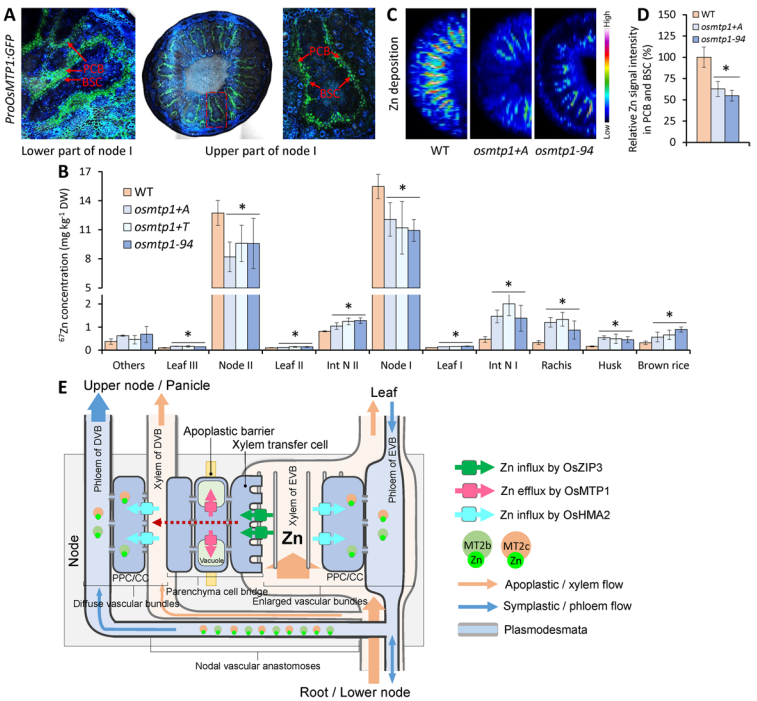

Fig. 2 Effect of *OsMTP1* knockout on Zn accumulation and the schematic representation of Zn transport in node. **A** GFP localization in the transverse section of node I in the transgenic lines carrying *ProOsMTP1:GFP*. Parenchyma cell bridge, PCB; bundle sheath cells, BSC. **B** Short-term labeling experiment of ^{67}Zn. ^{67}Zn concentration was shown in different organs of wild-type and *osmtp1* mutants. Plants grown in a 1/2 Kimura B solution until the filling stage were transferred to a solution containing 0.4 μM ^{67}Zn, 1 μM Rb and 1 μM Sr. After 2 d, different organs were sampled and subjected to element determination by ICP-MS. Internode, Int N. **C**, **D** Zn deposition (C) and relative Zn signal intensity in PCB and bundle sheath cells (BSC) (D) in the transverse section of node I in wild-type and *osmtp1* mutants at the filling stage. The accumulation of Zn was measured by LA-ICP-MS. The relative Zn signal intensity was estimated based on the gray value by Photoshop. Data are means ± SD ($n = 4$ in B; 6 in D). Asterisks above bars indicate significant differences compared to WT ($P < 0.05$, Tukey's test). **E** Schematic representation of Zn transport in node. OsZIP3 mediates Zn influx from EVB xylem to PCB, OsMTP1 mediates Zn efflux from cytosol to vacuole resulting in high Zn deposition in PCB and BSC, OsHMA2 mediates Zn influx from xylem to phloem in both EVB and DVB, and OsMT2b/2c binding Zn mediates Zn translocation in phloem

trichome formation in epidermal cells [48], showed expression patterns similar to the top two markers of Cluster 8. Furthermore, the enriched genes of Cluster 8 showed the highest correlation with the reported-enriched genes of epidermal cells from rice tissues of different organs [49], suggesting Cluster 8 may represent epidermal cells (Fig. 1C, E, Additional file 1: Fig. S4). (11) *OsCOMT*, enriched in Cluster 4 (Additional file 2: Table S2), and *OsCAD2*, expressed highly in sclerenchyma cells as confirmed by *Promoter:GUS* transgenic lines previously [50, 51], matched the top two markers of Cluster 4. The enriched genes of Cluster 4 showed the highest correlation with the reported-enriched genes of sclerenchyma [49], indicating Cluster 4 may be sclerenchyma identity (Fig. 1C, E, Additional file 1: Fig. S4).

Gene expression profile of transporters in rice node I

To clarify the expression profile of transporter genes in rice node, 1,144 putative transporter genes were obtained from the ARAMEMNON database (https://aramemnon.

botanik.uni-koeln.de/index.ep). Eight hundred eighty-seven transporter genes showed varied expression levels in the 11 cell types of node I (Additional file 2: Table S3), indicating that they exhibited differential roles in various cell types. While 256 transporter genes were not detected in the snRNA-seq (Additional file 2: Table S3), suggesting probable minor roles in node I.

Identification of candidate transporter genes for ions deposition in rice node

Elements showed varied deposition patterns in node I through spatial ionomics analysis using laser ablation-ICP-MS (LA-ICP-MS) (Additional file 1: Fig. S6A). Fe was highly deposited in PCB and parenchyma cells (Additional file 1: Fig. S6A), which has been reported to be associated with *OsVIT2* encoding a tonoplast-localized transporter for Fe accumulation in vacuole [52]. *OsVIT2* showed high expression in PCB [52], consistent with snRNA-seq data (Additional file 1: Fig. S6B, C). *OsVIT2* also showed some expression in parenchyma cells and sclerenchyma cells, with high correlation with Fe deposition in various tissues (Additional file 1: Fig. S6E).

In contrast, Zn was specifically and highly accumulated around PCB (Fig. 2C, Additional file 1: Fig. S6A). The tonoplast-localized OsMTP1, sequestrating Zn into vacuole [53], showed high gene expression in PCB and bundle sheath cells (Fig. 1C, Additional file 1: Fig. S4, S6B). There was a good correlation ($R^2 = 0.6231$) between *OsMTP1* expression and Zn deposition in various tissues in node I (Additional file 1: Fig. S6E), while its exact role in Zn deposition in node was unclear. The *ProOsMTP1:GFP* transgenic lines were used to confirm its high expression in PCB and bundle sheath cells (Fig. 2A). Furthermore, *osmtp1* mutants showed significantly decreased ^{67}Zn concentration in nodes (Fig. 2B), especially in PCB and bundle sheath cells (Fig. 2C, D), but significantly high Zn concentration in leaves, internodes, and panicles compared to WT (Fig. 2B). By contrast, *OsMTP1* knockout did not affect the accumulation of Rb and Sr (Additional file 1: Fig. S7), serving as the negative control. These results indicated that OsMTP1 plays key roles in high deposition of Zn in PCB and bundle sheath cells, as well as for Zn distribution from nodes to other organs, together with OsZIP3, OsHMA2, OsMT2b, and OsMT2c (Fig. 2E).

OsSPX-MFS3, OsHMA4, OsMTP8.1 and OsABCC1 are the key tonoplast-localized transporters for sequestrating P, Cu, Mn and As into vacuole [24, 54–57], respectively. *OsSPX-MFS3* was primarily expressed in PCB, and *OsHMA4* was highly expressed in DVB/TVB xylem, NVA and PCB (Additional file 1: Fig. S6B, C). *OsMTP8.1* showed high levels in cells of sclerenchyma, parenchyma and epidermis (Additional file 1: Fig. S6B, C), which was confirmed by immunostaining (Additional file 1: Fig. S6D). *OsABCC1* was mainly expressed in EVB phloem (Additional file 1: Fig. S6B, C), consistent with the previous study [55]. There was a good positive correlation with $R^2 > 0.5$ between the four genes expression and element accumulation in various tissues of node I (Additional file 1: Fig. S6E), respectively. These results suggested that the tonoplast-localized transporters for vacuolar ions accumulation play key roles in element deposition within rice node.

Identification and expression pattern of *OsMTP7*

The cation diffusion facilitator (CDF)/metal tolerance protein (MTP) family plays important roles in Mn or Zn transport in plants [19, 58]. Ten MTP members were found

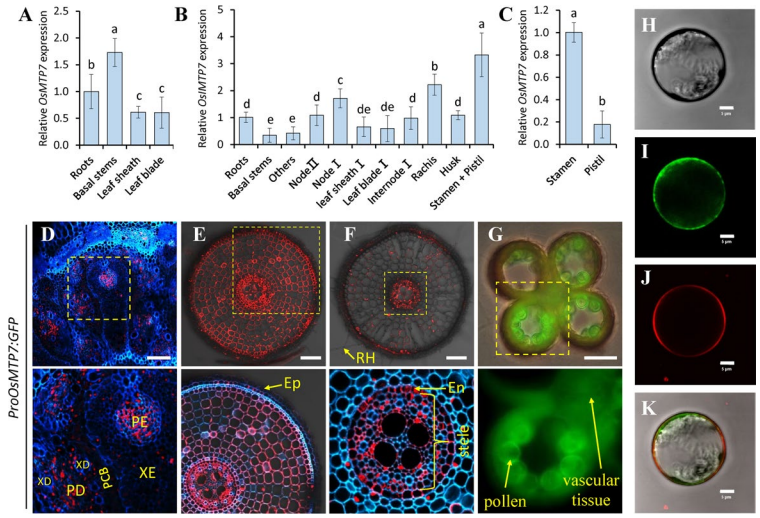

Fig. 3 Gene expression pattern and subcellular localization of OsMTP7. **A**-**C** Relative expression of *OsMTP7* in various organs of rice at the vegetative stage (**A**) and flowering stage (**B** and **C**). *Tubulin* was used as an internal standard. The expression level was determined using quantitative RT-PCR. Expression level relative to roots (**A** and **B**) or stamen (**C**) is shown. Data are means ± SD ($n = 3$). Different letters above bars indicate significant differences ($P < 0.05$, Tukey's test). **D**-**G** Tissue-specific expression of *OsMTP7*. Immunostaining with a GFP antibody was performed in the node I (**D**), main root tip (**E**), basal root zone (**F**), and the GFP fluorescence was detected in the anther (**G**) in the transgenic lines carrying *ProOsMTP7:GFP*. Red color indicates the GFP antibody-specific signal and blue color indicates cell wall autofluorescence (**D**-**F**). Phloem area of enlarged vascular bundle (PE), phloem area of diffuse vascular bundle (PD), xylem area of enlarged vascular bundle (XE), xylem area of diffuse vascular bundle (XD), parenchyma cell bridge (PCB), epidermis (Ep), root hair (RH), and endodermis (En) are shown. Bars, 100 μm. **H**-**K** Subcellular localization of OsMTP7. Construct of *35S:GFP-OsMTP7* was transiently expressed in the protoplasts prepared from rice shoots. FM4-64 was used as a plasma membrane-localized marker (**J**). Bright field (**H**), GFP image (**I**), FM4-64 image (**J**), and merged image (**K**) are shown. Bars, 5 μm

in rice (Additional file 1: Fig. S8, S9A, Additional file 2: Table S3). Except for the high expression of *OsMTP1* in PCB (Cluster 1) as its enriched gene (Figs. 1C, 2A, Additional file 1: Fig. S4), *OsMTP9* and *OsMTP7* were the enriched genes of bundle sheath cells (Cluster 5) and phloem of DVB/TVB (Cluster 0) in node I (Fig. 1C, Additional file 1: Fig. S4), respectively. The high expression of OsMTP9 in bundle sheath cells and PCB was confirmed by immunostaining (Additional file 1: Fig. S10). OsMTP1 and OsMTP9 mediated Zn or Mn transport, which play key roles in Zn and Mn homeostasis in rice (Fig. 2) [22, 53], respectively, while the role of *OsMTP7* remains unknown.

The cloned open reading frame (ORF) of *OsMTP7* contained 1,419 bp, encoding a peptide with 472 amino acids containing four putative transmembrane domains (Additional file 1: Fig. S9B, C). *OsMTP7* was highly expressed in the basal stems and roots at the vegetative stage (Fig. 3A), and in the flowers (stamen + pistil), rachis, and node I at the flowering stage (Fig. 3B). Furthermore, *OsMTP7* showed a five times higher level in the stamen than in the pistil (Fig. 3C). The expression of *OsMTP7* in roots was hardly affected by the deficiency or excess of Mn, Zn, Cu, or Cd (Additional file 1: Fig. S11A).

To confirm the tissue expression of *OsMTP7*, the transgenic rice lines expressing GFP driven by *OsMTP7* promoter were employed for immunostaining with an antibody against GFP. Consistent with the snRNA-seq data with enrichment in clusters 0 and 9 (Fig. 1C, Additional file 1: Fig. S4), a strong GFP signal was detected in the phloem

region of DVB and EVB in node I (Fig. 3D), which was further confirmed by qRT-PCR using four types of tissues of node I separated by laser microdissection (LMD) (Additional file 1: Fig. S11B). Additionally, GFP signal was highly detected in all cells except the epidermis in the root tip (Fig. 3E). Some GFP signal was found in the exodermis, sclerenchyma, and cortex in the basal root, but the strong GFP signal was observed in the endodermis and stele cells (Fig. 3F). Besides, a strong GFP fluorescence was detected in the pollen and vascular tissues of anther (Fig. 3G). In contrast, no GFP signal was detected in the root, node I, and anther of the WT plants (Additional file 1: Fig. S11C-E). These results implicated that *OsMTP7* was constitutively expressed in rice and may play roles in root, phloem of node, and stamen.

Subcellular localization of OsMTP7

The subcellular localization of OsMTP7 was analyzed by transiently expressing *OsMTP7-GFP* and *GFP-OsMTP7* in rice protoplasts. The signal of OsMTP7-GFP and GFP-OsMTP7 were localized to the cell periphery of the protoplast, and were highly co-localized with the plasma membrane markers including FM4-64 (Fig. 3H-K, Additional file 1: Fig. S12E-H) and AtPIP2a-mCherry (Additional file 1: Fig. S12M-T) [59]. In contrast, the signal of GFP alone was mainly localized to the cytosol and nuclei and hardly co-localized with that of FM4-64 and AtPIP2a-mCherry (Additional file 1: Fig. S12A-D, I-L). The results indicated that OsMTP7 was localized to plasma membrane in rice.

Effect of *OsMTP7* knockout on Mn homeostasis

To investigate the physiological role of *OsMTP7* in rice, three independent knockout lines of *OsMTP7*, *osmtp7-1* (one G deletion at target 1), *osmtp7-2* (one T insertion at target 2), and *osmtp7-3* (35 bp fragment deletion at target 2), were generated using CRISPR/Cas9 technology (Additional file 1: Fig. S13A). Knockout of *OsMTP7* hardly affected panicle number, but significantly inhibited plant height and dramatically reduced the dry weight of straw by 38%, panicles by 68%, and grains by 53%, as well as the fertility by 60% compared to WT at the repining stage grown in soil (Fig. 4A, Additional file 1: Fig. S13B-K). Remarkably, three *osmtp7* mutants showed greatly lower Mn concentrations in the nodes, leaf sheaths, leaf blades, and total straw by 39% and brown rice by 17% (Fig. 4B, C, Additional file 1: Fig. S14C, D), but comparable concentrations of Fe, Cu, and Zn in the straw and brown rice compared to WT through ionomics analysis using ICP-MS (Additional file 1: Fig. S14). Furthermore, the distribution of Mn was significantly higher in the nodes and leaf blades and dramatically lower in the grains of *osmtp7* mutants compared to WT (Fig. 4D).

To reveal how *OsMTP7* is involved in plant growth and Mn accumulation, hydroponic experiments were conducted. Under normal 0.5 μM Mn condition, significantly shorter leaf 8 (youngest), as well as dramatically lower dry weight of root, basal stems, and leaf 8 were observed in *osmtp7* mutants compared to WT (Fig. 4E, F). Ionomics analysis demonstrated that *OsMTP7* knockout significantly decreased Mn concentration in all examined organs compared to WT (Fig. 4G), which was consistent with the inhibited total Mn uptake via root by 13% and decreased Mn concentration in xylem sap by 31% (Fig. 4I, J). Furthermore, *OsMTP7* knockout increased Mn distribution in the old leaves 4–6 but dramatically decreased Mn allocation in the youngest leaf 8 compared to WT

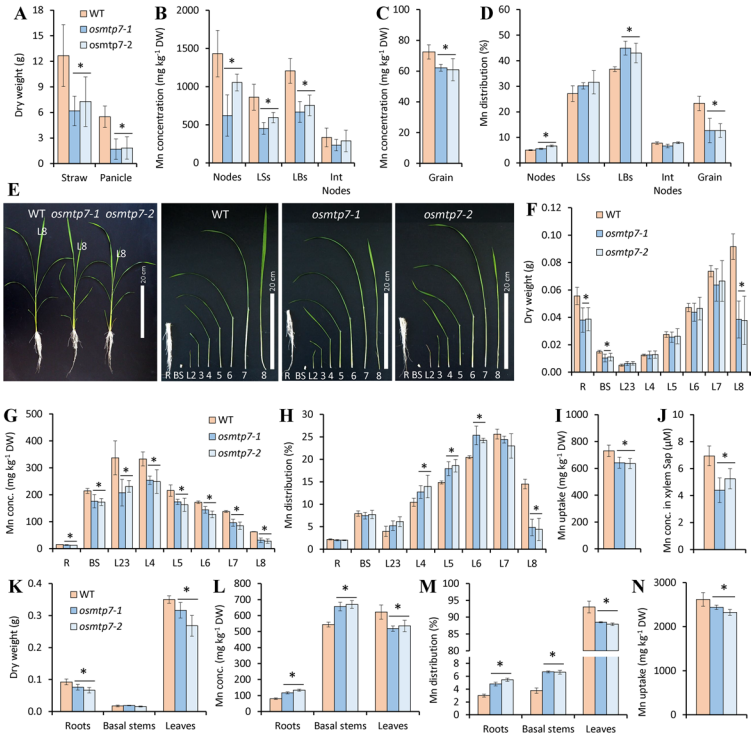

Fig. 4 Effect of *OsMTP7* knockout on plant growth and Mn homeostasis. **A**-**D** Plant growth and Mn homeostasis at the ripening stage. Dry weight of straw and panicle (**A**), Mn concentration in various organs (node, leaf sheath, leaf blade, and inter node) of straw (**B**) and grain (**C**), and Mn distribution in various organs (**D**) in wild-type and *osmtp7* mutants. Plants were grown in the potted soil and sampled at the ripening stage. Element concentration was determined using ICP-MS. **E**-**N** Plant growth and Mn homeostasis at the vegetative stage. Phenotype of plants and various organs (**E**), dry weight (**F**, **K**), Mn concentration (**G**, **L**), and Mn distribution (**H**, **M**) in various organs (roots, basal stems, leaf 2–8, or leaves), Mn uptake (**I**, **N**), and Mn concentration in the xylem sap (**J**) in wild-type and *osmtp7* mutants. Plants were grown in a ½ Kimura B solution containing normal Mn with 0.5 μM for 6 weeks (**E**-**J**) or increased Mn with 5 μM for 4 weeks (**K**-**N**). Bars = 20 cm in (**E**). Data are means ± SD ($n = 5$ in **A**-**D**; 4 in **F**-**J**; 3 in **K**-**N**). Asterisks above bars indicate significant differences compared to WT ($P < 0.05$, Tukey's test)

(Fig. 4H). Besides, *OsMTP7* knockout hardly affected Fe concentration in the examined organs, but partially decreased Cu or Zn concentrations in some leaves and partially increased Zn concentration in the roots (Additional file 1: Fig. S15A-C). The uptake of Fe, Cu, or Zn was comparable among the genotypes (Additional file 1: Fig. S15D-F).

To get rid of the effect of other Mn transporters in *osmtp7* mutants, the expression of *OsNRAMP5*, *OsNRAMP1*, *OsMTP9*, *OsNRAMP3*, and *OsYSL2*, involved in Mn uptake and translocation [21–23, 28, 30], and *OsYSL6*, *OsMTP8.1*, and *OsMTP8.2*, involved in Mn detoxification [24, 25, 29], were analyzed. *OsMTP7* knockout did not alter the expression of the eight genes in the roots (Additional file 1: Fig. S16), implying the direct involvement of *OsMTP7* in Mn homeostasis in rice.

Furthermore, under a high 5 μM Mn condition, lower dry weight of roots and leaves (Fig. 4K) and lower Mn uptake (Fig. 4N) were also found in *osmtp7* mutants compared to WT. While significantly increased Mn concentration and distribution in roots and basal stems, and significantly decreased Mn concentration and distribution in leaves were detected in *osmtp7* mutants compared to WT (Fig. 4L, M). These results indicated that rice *OsMTP7* plays important roles in Mn uptake via root, Mn translocation from root to shoot

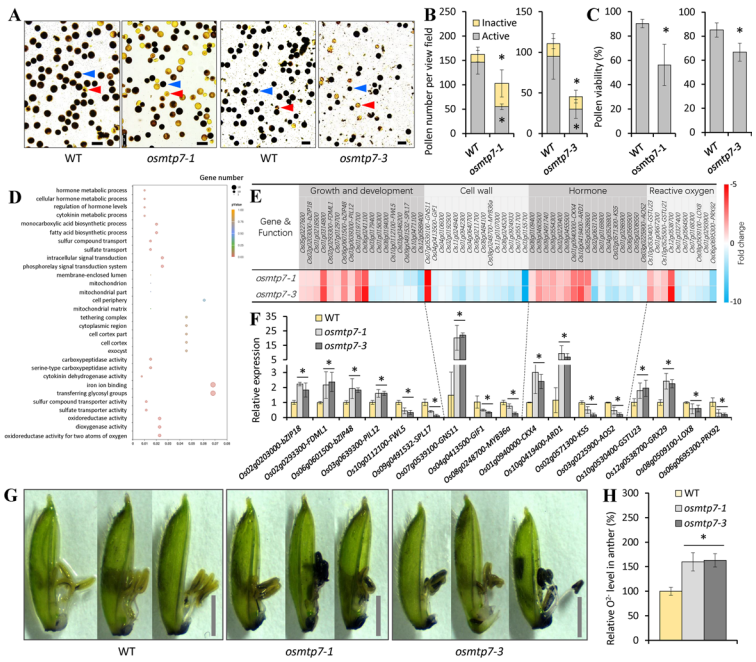

Fig. 5 Effect of *OsMTP7* knockout on fertility at the flowering stage. **A**-**C** Pollen viability determination. Pollen staining by 1% KI–I_2 (**A**) and pollen number in each same view field (**B**), and pollen viability (**C**) in wild-type and *osmtp7* mutants. Blue arrowhead indicates normal pollen (black color), and red arrowhead indicates abnormal pollen (yellow color). **D**-**F** Bulk RNA-seq analysis of spikelets before flowering. Gene ontology (GO) analysis of differentially expressed genes (DEGs), hierarchical clustering and expression heatmap of selected DEGs (**E**), and DEGs validation by qRT-PCR for 17 genes (**F**) in wild-type and *osmtp7* mutants (**D**). **G**-**H** O^{2-} staining (**G**) and relative O^{2-} level (**H**) in anther of wild-type and *osmtp7* mutants. The spikelets were sampled before flowering to stain O^{2-} using nitroblue tetrazolium (NBT). The relative O^{2-} level in anther was estimated based on the gray value by Photoshop. Plants were grown in the potted soil and sampled at the flowering stage. Bars = 100 μm in (**A**); 2 mm in (**G**). Data are means ± SD ($n = 5$ in **B** and **C**; 3 in **F**; 9 in **H**). Asterisks above bars indicate significant differences compared to WT ($P < 0.05$, Tukey's test)

through xylem especially in high Mn condition, and Mn distribution from nodes and old leaves to new leaf and grain via nodes, which is crucial for plant growth and yield.

Role of *OsMTP7* in fertility

Due to the extremely decreased fertility in *osmtp7* mutants and the high expression of *OsMTP7* in stamen (Fig. 3B, C, Additional file 1: Fig. S13F, I), the anther growth and pollen viability were compared among the genotypes. *osmtp7* mutants showed partially distorted anthers (Additional file 1: Fig. S17A) and dramatically lower pollen number and pollen viability (Fig. 5A-C) compared to WT. To understand the mechanism underlying the low fertility of *osmtp7* mutants, bulk RNA-seq analysis was conducted using the spikelets of WT and *osmtp7* mutants. 322 upregulated genes and 472 downregulated genes were identified in both *osmtp7* lines compared to WT (Additional file 1: Fig. S17B, C). Gene ontology (GO) analysis revealed enrichment in processes such as oxidoreductase activity, nutrition metabolism, hormone metabolism, mitochondrion activity, etc. (Fig. 5D). Four selected groups of genes, involved in plant growth and development, the synthesis and metabolic processes of cell wall, hormone and reactive oxygen, were

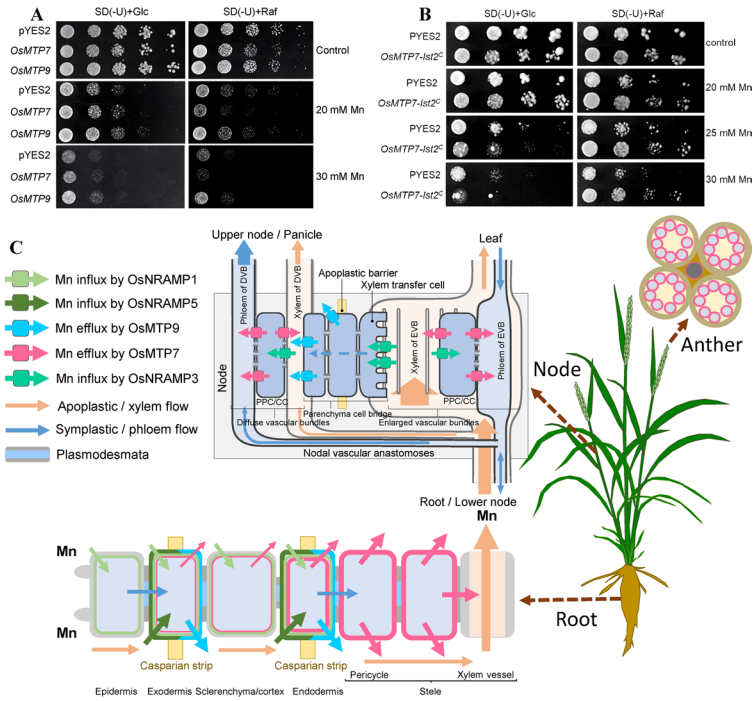

Fig. 6 Transport activity of OsMTP7 in yeast and the schematic representation of Mn transporters in rice. **A**, **B** Transport activity of OsMTP7 for Mn in yeast. The yeast carrying pYES2 empty vector, *pYES2-OsMTP7*, *pYES2-OsMTP9*, or *pYES2-OsMTP7-Ist2*^{C} was cultured on a SD-U medium plate with glucose or raffinose containing 20, 25 or 30 mM $MnCl_2$ for 2 or 3 d. **C** Schematic representation of Mn transporters in root, node and anther of rice. *OsMTP7* is expressed highly in endodermis and stele cells of root, phloem cells in node, and pollen and vascular tissue in anther. OsMTP7 is a plasma membrane-localized transporter for Mn efflux. OsMTP7 is involved in Mn uptake, translocation from root to shoot through xylem, and phloem loading for distribution in node, which is important for plant growth and fertility in rice. Besides, OsNRAMP1/3/5 mediate Mn influx and OsMTP9 mediates Mn efflux in root and node

shown (Fig. 5E). The expression of 17 reported or putative genes for the above four functions were further confirmed through qRT-PCR (Fig. 5F) [60–71].

Since the genes for oxidoreductase activity were affected (Fig. 5D, E), Mn functions in Mn-SOD for reactive oxygen species (ROS) scavenging, and the fine ROS homeostasis is crucial for fertility [72–74], the superoxide anion (O^{2-}) level in the spikelets was determined. A significantly higher level of O^{2-} in the anthers was observed in *osmtp7* mutants than in the WT (Fig. 5G, H). These results indicated that knockout of *OsMTP7* disturbed genes expression involved in synthesis and metabolic processes for growth and development in spikelets, leading to increased ROS level and oxidative stress in anther, resulting in low fertility and yield loss.

Transport activity test of OsMTP7 for elements in yeast

To investigate the transport activity of OsMTP7 for elements, *OsMTP7* was expressed in yeast. OsMTP9, the plasma membrane-localized Mn efflux transporter [22], was employed as the positive control. The yeast cells carrying pYES2 empty vector, pYES2-*OsMTP7*, or pYES2-*OsMTP9* showed similar growth on the plate of control or glucose (Fig. 6A, B). While on the plates containing raffinose and high Mn, the yeast cells

carrying *OsMTP9* showed better growth than that carrying pYES2 (Fig. 6A), consistent with the previous report [22]. Unexpectedly, the yeast cells carrying *OsMTP7* showed increased sensitivity to high Mn compared to that carrying pYES2 (Fig. 6A). Since the mislocalization of the transporter in yeast could affect the yeast growth phenotype under metal stress [54, 75], the subcellular localization of OsMTP7 in yeast was investigated. GFP-OsMTP7 was found to be localized to the inner membrane in yeast (Additional file 1: Fig. S18A), different from the plasma membrane localization of OsMTP7 in rice (Fig. 3I, Additional file 1: Fig. S12). To direct OsMTP7 to yeast plasma membrane, OsMTP7 was fused with the soluble C-terminal domain of Ist2p ($Ist2^C$), a dominant driving protein to plasma membrane (Additional file 1: Fig. S18B) [76]. The yeast cells carrying *OsMTP7-Ist2*^{C} showed increased tolerance to high Mn compared to that carrying pYES2 under raffinose-induced condition (Fig. 6B). On the other hand, expression of *OsMTP7* or *OsMTP7-Ist2*^{C} in yeast hardly affected the tolerance to Cu, Fe and Zn (Additional file 1: Fig. S19), consistent with no difference in their concentration between *osmtp7* mutants and WT (Additional file 1: Fig. S14). These results indicated that OsMTP7 probably shows efflux transport activity for Mn, but not Cu, Fe and Zn.

Discussion

Rice nodes contain complex tissues and well-organized vascular systems. Several key tissues, such as EVB, TVB, DVB, SVB, PCB and NVA, have been identified based on the anatomical morphology analysis [2, 3, 8]. We here used snRNA-seq to identify 11 distinct cell clusters at the single-cell resolution depending on 1,837 cluster-enriched genes in node I, and further annotated each cell type depending on the marker or enriched genes (Fig. 1, Additional file 1: Fig. S1-4, Additional file 2: Table S2). Although a lack of true biological replicates for each growth stage, the marker or enriched gene expression patterns from snRNA-seq were highly consistent with that of the reported or newly confirmed genes in node (Figs. 1, 2, 3, Additional file 1: Fig. S5-6, S10-11), confirming the high reliability of snRNA-seq data. While other sub-cell clusters could be further divided in the future through additional biological replicates and in-depth data mining, such as cluster 0/phloem of DVB/TVB, cluster 2/xylem of DVB/TVB, and cluster 4/sclerenchyma cells (Fig. 1), which would further promote the studies of the cellular developmental trajectories [32, 33]. Importantly, rice node acts as a hub for distributing mineral elements depending on various transporters [2, 3], while the expression pattern and the role of most of them in node are uncovered. We here systematically profiled the expression patterns of 1,144 putative transporter genes across 11 cell types (Additional file 2:Table S3), although 256 of them were not detected, which will serve as an important database for identifying key genes in node.

Rice nodes not only accumulate high concentration of elements [44, 55, 77], but also show specific deposition patterns for differential elements (Additional file 1: Fig. S6) [78, 79], which is important for the storage and reutilization of elements. We found that the expression patterns of *OsMTP1*, *OsVIT2*, *OsSPX-MFS3*, *OsHMA4*, *OsMTP8.1* and *OsABCC1*, which encoding the tonoplast-localized transporter for vacuolar ions accumulation [24, 52–57], showed strong correlation with the specific deposition patterns of Zn, Fe, P, Cu, Mn and As in differential tissues in node I (Fig. 2, Additional file 1: Fig. S6), respectively. Knockout of *OsMTP1* or *OsVIT2* confirmed its key role in Zn or Fe

deposition around PCB (Fig. 2) [52], respectively, indicating the important role of transporters for vacuolar ions accumulation in the deposition patterns of elements in rice node. On the other hand, knockout of *OsMTP1* or *OsVIT2* greatly increased Zn or Fe concentration in grain because of the decreased Zn or Fe accumulation in nodes (Fig. 2) [52, 53], suggesting that our data will provide candidate genes for rice breeding with higher mineral nutrients and lower toxic elements.

CDF/MTP members in rice and Arabidopsis were divided into two subgroups. OsMTP7 belonged to the clade together with OsMTP8.1, OsMTP8.2, AtMTP8, OsMTP9, OsMTP11, and AtMTP11 (Additional file 1: Fig. S9A), which have been reported to mediate Mn efflux from cytosol [22, 24, 26, 80–82]. OsMTP7 was localized to plasma membrane in rice (Fig. 3H-K, Additional file 1: Fig. S12), and the localization of OsMTP7 to plasma membrane in yeast resulted in increased tolerance to high Mn (Fig. 6B, Additional file 1: Fig. S18B), similar to the role of OsMTP9 in yeast (Fig. 6A) [22], suggesting its probable efflux ability for Mn (Fig. 6C). Besides, OsMTP7 likely showed no transport activity for Cu, Fe and Zn (Additional file 1: Fig. S14, S19). In rice roots, *OsNRAMP5* and *OsMTP9* were specifically expressed in exodermis and endodermis cells (Fig. 6C) [21, 22], and *OsNRAMP1* was expressed in the cells except for stele cells (Fig. 6C) [23]. In contrast, *OsMTP7* was likely a novel Mn efflux transporter gene that was highly expressed in stele cells (Figs. 3F, 6C). Additionally, *OsMTP7* was also expressed in almost all cells in main root tip and partially in other cells in root basal zone (Figs. 3E, F, 6C). The polarly localized OsNRAMP5 and OsMTP9 have been suggested to compose the effective Mn uptake system in rice with the supplement of OsNRAMP1 (Fig. 6C) [21–23]. Knockout of *OsMTP7* did not alter the expression levels of *OsNRAMP5*, *OsNRAMP1*, *OsMTP9*, and other Mn transporter genes in roots (Additional file 1: Fig. S16), hardly affected the Fe, Cu and Zn accumulation (Additional file 1: Fig. S14), but decreased Mn uptake, Mn concentration in xylem sap and Mn translocation from roots to leaves (Fig. 4), resulting in greatly decreased Mn concentration in roots, leaves, straw, and grain (Fig. 4, Additional file 1: Fig. S14C, D). These results indicated that OsMTP7 plays important roles in the uptake, radial transport, and root-to-shoot translocation of Mn in roots (Fig. 6C).

OsMTP7 was highly expressed in phloem region of both EVB and DVB in rice node (Figs. 1C, 3D). Knockout of *OsMTP7* decreased Mn distribution from basal stems to leaves and from old leaves to the newest leaf at the vegetative stage, and from nodes and leaves to grains at the reproductive stage (Fig. 4D, H). The effect of *OsMTP7* on Mn distribution was similar as *OsNRAMP3* on Mn distribution (Fig. 6C, Additional file 1: Fig. S20) [30], OsHMA2 and OsMT2b/2c on Zn distribution [17, 44], and OsYSL16 on Cu distribution [83] through phloem in node, indicating that OsMTP7 was involved in mediating Mn distribution in nodes by loading Mn to the phloem of EVB and DVB (Fig. 6C). Additionally, *OsMTP9*, encoding efflux transporter for Mn in root exodermis and endodermis cells [22], was detected to be expressed primally in PCB and bundle sheath cells in node I (Fig. 1C, Additional file 1: Fig. S10), suggesting that OsMTP9 may be involved in Mn efflux from bundle sheath cells and PCB to DVB for the inter-vascular transfer of Mn (Fig. 6C), though further research is required to confirm this hypothesis.

Knockout of *OsNRAMP5*, *OsNRAMP1*, *OsMTP9* or *OsNRAMP3* resulted in inhibited growth or low fertility [21–23, 30]. Similarly, *OsMTP7* knockout reduced growth,

fertility and production, which could be attributed to Mn deficiency in the roots, leaves, straw, and grain (Fig. 4, Additional file 1: Fig. S13-14). Although the exact reasons for the inhibition in mutants of *OsNRAMP1/3/5* and *OsMTP7/9* might vary, decreased PSII quantum yield was found in *osmtp9* mutants [22], indicating that Mn deficiency-induced photosynthesis inhibition may be the cause, because Mn acts as a cofactor in PSII supercomplex. Besides, the decreased fertility in *osmtp7* mutants was presumably a combination of the retarded anther development and inhibited pollen viability (Fig. 5A-C, Additional file 1: Fig. S17A), where *OsMTP7* was highly expressed (Fig. 3B, C, G). Further research through bulk RNA-seq using spikelets revealed that *OsMTP7* knockout altered the expression of genes involved in multiple processes, which were important for plant growth and development, the synthesis and metabolic processes of cell wall, hormone and reactive oxygen (Fig. 5D-F) [60–71]. This altered gene expression profile was consistent with the defects in the biosynthesis and deposition of cell wall polysaccharides and ROS homeostasis resulted from disturbed Mn homeostasis in the previous studies [27, 84–86]. Moreover, increased ROS level and oxidative stress in the anther of *osmtp7* mutants were confirmed (Fig. 5G, H), which may be attributed to the inhibited Mn-SOD ability that is important for ROS scavenging [72].

Conclusions

This study identifies 11 distinct cell clusters at the single-cell resolution in rice node I using snRNA-seq, and annotates each cell type through multiple marker or enriched genes. This study provides the expression profile of various transporter genes in the 11 cell clusters, and candidate transporter genes for the varied deposition patterns of multiple elements in rice node I, which will serve as an important database for identifying key genes in node. Furthermore, this study identifies *OsMTP7* as a novel Mn efflux transporter gene that is highly expressed in node phloem and root stele cells. OsMTP7 mediates Mn uptake, translocation and distribution for improving growth and yield in rice.

Methods

Plant materials and hydroponic conditions

Wild-type (WT) rice (*Oryza sativa* cv. Nipponbare), the transgenic lines carrying *ProOsPHO1;1:GFP*, *ProOsMT2c:GFP*, *ProOsMTP1:GFP*, or *ProOsMTP7:GFP*, and three independent knockout lines of *OsMTP1* or *OsMTP7* generated as described below, were used in this study. Seeds were soaked in water in the dark at 30 °C for 2–3 d for germination and were then placed on a plastic net floating on a 0.5 mM $CaCl_2$ solution (pH 5.6). After 5 d, the seedlings were transferred to ½ Kimura B solution (pH 5.6) in a plastic pot. The nutrient solution was changed every 3 d. Plants were grown in a controlled greenhouse at 25–35 °C with natural sunlight in Kurashiki, Japan, or Kunming, China.

The ½ Kimura B solution contained macronutrients (mM) including $(NH_4)_2SO_4$ (0.18), $MgSO_4{\cdot}7H_2O$ (0.27), KNO_3 (0.09), $Ca(NO_3)_2{\cdot}4H_2O$ (0.18), and KH_2PO_4 (0.09), and the micronutrients (μM) including $MnCl_2{\cdot}4H_2O$ (0.5), H_3BO_3 (3.0), $(NH_4)_6Mo_7O_{24}{\cdot}4H_2O$ (1.0), $ZnSO_4{\cdot}7H_2O$ (0.4), $CuSO_4{\cdot}5H_2O$ (0.2), and Fe-EDTA (20) [87].

Preparation of node I samples and nucleus isolation

Segments of Node I were precisely excised using a sterile razor blade from over 20 individual rice (cv. Nipponbare) plants grown in ½ Kimura B solution at the booting stage (RNA3), flowering stage (RNA2), and filling stage (RNA1), respectively. The harvested node I samples were immediately immersed in ice-cold water and maintained on ice to preserve cellular integrity before subsequent nuclear isolation and fluorescence-activated nucleus sorting, as previously described [88–90]. Briefly, plant tissue samples were collected and cut into small pieces (< 0.5 cm) and then homogenized using a glass Dounce tissue grinder (Sigma, cat. no. D8938) in an ice-cold nucleus lysis buffer. The tissue was homogenized with pestle A for 25 strokes, followed by 25 strokes with pestle B in 2 mL of the lysis buffer. The homogenate was incubated on ice for 5 min, after which an additional 3 mL of cold EZ lysis buffer was added, and the sample was further incubated on ice for another 5 min to ensure complete nuclear release. The sample was then centrifuged at 500 g for 5 min at 4 °C to pellet the nucleus. The resulting nucleus pellet was washed with 5 mL of ice-cold EZ lysis buffer and incubated on ice for an additional 5 min. After centrifugation, the pellet was resuspended in 5 mL of nucleus suspension buffer (NSB, containing 1 × PBS, 0.01% BSA, and 0.1% RNase inhibitor (Clontech, cat. no. 2313 A). The suspension was filtered through a 35 μm cell strainer (Corning-Falcon, cat. no. 352235) to remove any debris. Nuclei were then counted using a hemocytometer. Finally, the suspension was adjusted to a concentration of 1,000 nuclei/μL for loading onto a 10 × Genomics platform.

SnRNA-seq library preparation and sequencing

SnRNA-seq libraries were prepared using the Chromium Next GEM Single Cell 3' Reagent Kits v3.1 (10 × Genomics) on a Chromium Controller. Nuclei were isolated from node I and resuspended in PBS containing 0.04% BSA. Nuclei from each developmental stage were separately loaded onto the Chromium Next GEM Chip G to generate single-cell gel beads in emulsion (GEMs), according to the manufacturer's instructions. The captured nuclei were subsequently lysed, and the released RNA underwent reverse transcription to produce barcoded, full-length cDNA. Libraries were constructed following the protocol provided by the reagent kit. The quality of the libraries was assessed using the Qubit 4.0 Fluorometer and the Agilent 2100 Bioanalyzer. Sequencing was performed on the Illumina NovaSeq 6000 platform, achieving a sequencing depth of at least 50,000 reads per nucleus, with paired-end 150 bp (PE150) reads.

Data processing and dimensionality reduction for snRNA-seq of 10 × genomics

High-throughput single-nucleus transcriptome sequencing (snRNA-seq) of each rice node I sample was performed using the 10 × Genomics platform. Raw sequencing data were aligned to the rice (cv. Nipponbare) reference genome (T2T) (http://www.ricesuperpir.com/web/nip) using the STAR aligner [91], and adapter sequences and low-quality reads were filtered out using FASTP to ensure data quality. Cell barcodes were identified, and unique molecular identifiers (UMIs) were counted using UMI-TOOLS. Following alignment, Cell Ranger v7.0 was used for cell-calling to identify barcodes containing valid nuclei, which were further filtered to remove low-quality nuclei and potential doublets. Specifically, nuclei were retained if: (i) the number of detected genes

was between 500 and 7,000, (ii) the total UMI count per nucleus was ≥ 100. And genes expressed in at least ten nuclei were retained for downstream analysis.

Subsequently, differential expression analysis, clustering, and cell-type identification were performed in Seurat (v4.0.1). Gene expression values were normalized with the LogNormalize method, and the top 2,000 highly variable genes (HVGs) were selected. These HVGs were subjected to standardization before principal component analysis (PCA). The top 30 principal components (PCs) were used for nonlinear dimensionality reduction and visualization by t-distributed stochastic neighbor embedding (t-SNE) and uniform manifold approximation and projection (UMAP) [92, 93]. Clustering was performed using the shared nearest neighbor (SNN) modularity optimization algorithm.

Cluster-specific marker genes were identified using the FindAllMarkers function in Seurat. A gene was considered a marker if it was expressed in at least 25% of nuclei within the cluster, with $|\log_2$ fold change$| > 0.4$ and an adjusted p-value (q) ≤ 0.01.

RNA in situ hybridization

Sense and antisense RNA probes targeting the parenchyma cell marker gene *Os09g0333600* were synthesized in vitro using the Digoxigenin (DIG) RNA Labeling Kit (Roche), with the primer sequences listed in Additional file 2: Table S5, and applied to tissue sections for RNA in situ hybridization. Tissue samples consisted of node I collected at the flowering stage of rice (cv. Nipponbare). Paraffin-embedded Sects. (10 μm thick) and whole-mount preparations were subjected to RNA in situ hybridization according to previously published protocols [47, 94]. Hybridization was carried out at 50 °C for 16 h. After washing, the slides were incubated with an anti-digoxigenin antibody (Roche), the signal of which was then detected in the nitro-blue tetrazolium/5-bromo-4-chloro-30-indolyphosphate stock solution (NBT/BCIP solution; Roche).

Tissue-specific gene expression or protein localization determination

The transgenic lines carrying *ProOsMT2c:GFP* containing 2,040 bp fragment upstream of the ATG of *OsMT2c, ProOsMTP1:GFP* containing 4,566 bp fragment upstream of the ATG of *OsMTP1*, or *ProOsPHO1;1:GFP* containing 2.0 kb fragment upstream of the ATG of *OsPHO1;1* were constructed and used in previous studies [12, 44, 53]. To construct *ProOsMTP7:GFP* transgenic lines, genomic DNA of rice (cv. Nipponbare) was extracted using the phenol/chloroform method. The 2,514 bp fragment upstream of the ATG of *OsMTP7* was amplified by PCR from genomic DNA and then cloned into pPZP2H-lac carrying Green Fluorescent Protein (GFP) and the terminator of the nopaline synthase gene [95]. This construct was introduced into *Agrobacterium tumefaciens* (strain EHA101) for transformation into rice callus (cv. Nipponbare) [96]. The roots from plants grown in the hydroponic solution, and the node I and anthers from plants grown in soil were sampled and cut into slices using a vibrating slicer.

Immunostaining was performed using an antibody against GFP (A11122; Molecular Probes, MA, USA), OsLsi6, OsHMA5, OsHMA2, OsLsi2, OsLsi3, OsMTP8.1 or OsMTP9 as described previously [9, 13, 17, 22, 24]. The fluorescence of the secondary antibody (Alexa Fluor 555 goat anti-rabbit IgG, Molecular Probes) was recorded using a laser scanning microscope (Leica TCS SP8 X). GFP fluorescence in the anthers or node

I was observed using a laser scanning microscope. Primers used are listed in Additional file 2: Table S5.

Analysis of plant growth and mineral accumulation

In the hydroponic experiments, rice seedlings of WT, *osmtp1* or *osmtp7* mutants, generated as described below, were cultured in ½ Kimura B solution containing normal Mn with 0.5 μM for 6 weeks or increased Mn with 5 μM for 4 weeks, or grown in ½ Kimura B solution until the filling stage and then transferred to a solution containing 0.4 μM ^{67}Zn, 1 μM Rb and 1 μM Sr for 2 d. Various organs, including roots, basal stems, leaves, nodes, internodes, rachis, husk or brown rice, were sampled. To collect xylem sap, rice seedlings were grown in ½ Kimura B solution, the shoot (2 cm above the root) was removed with a razor, and the xylem sap was collected for 1 h using a micropipette.

In the potted soil experiments, rice seedlings were grown on the potted soil (3.5 L) in a closed glasshouse at 25–35 °C under natural sunlight. After ripening, the plant height and panicle number were recorded, and the shoot and panicle were photographed. The weights of the straw, panicles, and grains and the fertility were determined after drying in a 40 °C oven for several days, as described previously [97].

Concentrations of elements in each sample were determined using inductively coupled plasma MS (ICP-MS) after digestion as described in the following section. Uptake of element = elemental content in plant/root dry weight.

Spatial ionomics analysis through LA-ICP-MS

Node I was sampled at filling stage and element deposition was determined (two replicates) using laser ablation-ICP-MS (LA, NWR213, New Wave Research; ICP-MS 7700X, Agilent Technologies, CA, USA) based on previously described procedures [44, 79].

Clone of *OsMTP7*

Total RNA was extracted from rice (cv. Nipponbare) using a kit (Qiagen, http://www.qiagen.com; or Omega Bio-Tek, Norcross, GA, USA), and 500 ng of RNA was converted to cDNA using ReverTra Ace qPCR RT Master Mix (SuperScript II, Invitrogen). The full-length coding region of *OsMTP7* (*Os04g0298200* or *LOC_Os04g23180*) was amplified from cDNA using PCR and primers (Additional file 2: Table S5) that were designed based on the Rice Annotation Project database (RAP, http://rapdb.dna.affrc.go.jp/). The amplified fragment was cloned into a pGEM-T vector (Promega, https://www.promega.com/), and the sequence was confirmed using an ABI Prism 3130 sequence analyzer (Applied Biosystems, http://www.appliedbiosystems.com/).

Gene expression analysis

For analysis of *OsMTP7* expression in differential organs, various organs (roots, basal stems, leaf sheaths, leaf blades, internodes, nodes, rachises, husks, stamens, or pistils) were sampled from rice (cv. Nipponbare) grown on soil at the vegetative stage (4-w-old) and flowering stage (14-w-old). For the metal response analysis of *OsMTP7* expression

in the roots, rice seedlings (cv. Nipponbare) were exposed to ½ Kimura B solution with (CK) or without Mn, Zn, or Cu, or containing 200 μM $MnCl_2$, 100 μM $ZnSO_4$, 2 μM $CuSO_4$, or 1 μM $CdSO_4$. The roots were sampled for RNA extraction after 1 week. Tissue specific expression in node I was investigated using samples prepared by laser microdissection (Applied Biosystems Arcturus Laser Capture Microdissection System, Life Technologies, Carlsbad, CA, USA) as described previously [55]. For expression analysis of 8 genes involved in Mn homeostasis, the roots were sampled from plants grown in ½ Kimura B solution for 1 month. For expression analysis of 17 genes in spikelets, the spikelets were sampled from plants grown in soil before flowering. Total RNA and cDNA were prepared as described previously. *Tubulin* was used as the internal standard. Gene expression levels were determined using a kit (Thunderbird SYBR qPCR Mix, Toyobo, Osaka, Japan; or SuperReal PreMix Plus SYBR Green, Tiangen) and qRT-PCR (CFX96 Touch, Bio-Rad; or QuantStudio7 Flex, Applied Biosystems, Foster City, CA, USA). Primers used here were listed in Additional file 2: Table S5.

Subcellular localization

The open reading frame (ORF) of *OsMTP7* was cloned and ligated to the 5′ or 3′ end of *GFP* under CaMV35S promoter in pUC18 (Takara, Kyoto, Japan) as described previously [53, 54]. FM4-64 or AtPIP2a-mCherry was employed as a plasma membrane-localized marker [59]. The constructs were introduced into rice leaf protoplasts using the polyethylene glycol method [98]. The fluorescence signal was recorded using a laser scanning microscope (OLYMPVS, FV3000). Primers used here were listed in Additional file 2: Table S5.

Generation of rice mutants

The three *osmtp1* mutant lines were constructed through CRISPR/Cas9, which are loss-of-function mutants used in previous studies [53]. Two target sites of *OsMTP7* were designed using CRISPR-P v2.0 (http://crispr.hzau.edu.cn/cgi-bin/CRISPR2/CRISPR). The sequences were synthesized and cloned into the *Bbs* I-linearized pU6gRNA vector, respectively [99]. OsU3-gYSA in pZDgRNA-Cas9ver.2_HPT was replaced by the above synthetic gRNA construct using *Asc* I and *Pac* I restriction sites [99]. The final constructs were transformed into calluses (cv Nipponbare) through *Agrobacterium* transformation [96]. A genomic fragment was amplified from the transgenic rice plants using PCR and primer pairs flanking the designed target sites, and the amplified fragment was sequenced directly to identify the genotype of the mutants. T3 generations of three independent *osmtp7* mutants were used for the analysis as followed. Primer sequences were listed in Additional file 2: Table S5.

Analysis of flowers and pollen viability

Before flowering, fresh rice spikelets were collected and half the husk was removed for photographing with a microscope. For pollen viability measurement, the pollen grains from equal anthers of the genotypes were collected and stained with 1% KI-I_2 solution for 5 min, and then photographed under an optical microscope [44]. Black or yellow

color pollen was recorded as normal or abnormal pollen, respectively. Pollen viability ratio = pollen stained with black color/total pollen on the screen × 100.

Bulk RNA-seq analysis

The spikelets were sampled before flowering from wild-type rice and two *osmtp7* mutants grown in soil. RNA was extracted and assessed using RNA Nano 6000 Assay Kit of Bioanalyzer 2100 system (Agilent Technologies, CA, USA). Qualified RNA was used to construct cDNA library for RNA-Seq analysis on the Illumina HiSeq™ X TEN platform (Novogene Bioinformatics Technology Co., Ltd. -Tianjin, Beijing, China). The feature Counts v1.5.0-p3 was used to count read numbers mapped to each gene. The FPKM of each gene was calculated based on gene length and the read count mapped to it.

Histochemical assays of superoxide anion (O^{2-}) in anther

Before flowering, fresh rice spikelets were collected and stained with the solution (pH 7.8, 120 mM K_2HPO_4, 9 mM KH_2PO_4, 0.6 mM nitro blue tetrazolium, NBT) after removing half of the husk. After 1 h, the spikelets were washed with 95% alcohol and photographed under an optical microscope [73]. The relative O^{2-} level in the anthers was estimated based on the gray value using Photoshop.

Transport activity assay of OsMTP7 in yeast

The *OsMTP7*, *OsMTP9*, *GFP-OsMTP7*, or *GFP-OsMTP7-Ist2^C* was amplified by PCR using the primers listed in Additional file 2: Table S5 and then cloned into the pYES2 vector. The pYES2 empty vector, *pYES2-OsMTP7*, *pYES2-OsMTP9*, *pYES2-GFP-OsMTP7* or *pYES2-GFP-OsMTP7-Ist2^C* was transformed into yeast strain Δ*ycf1* for Mn and BY4741 for Cu, Fe and Zn. The yeast was grown in SD(-Uracil) solid medium containing 0.67% (w/v) yeast nitrogen base without amino acids (Difco), 2% (w/v) glucose, 0.2% (w/v) amino acids without uracil, and 2% (w/v) agar for selection. For the plate experiment, the yeast was cultured on SD-U medium plates with glucose or raffinose containing various $MnCl_2$, $FeSO_4$, $CuSO_4$ or $ZnSO_4$ for 2–4 d. The GFP fluorescence signal of GFP in yeast was recorded using a laser scanning microscope (OLYMPVS, FV3000).

Ionomics analysis through ICP-MS

The harvested samples were dried at 70 °C for 3 d or 50 °C for 7 d, and subjected to digestion using concentrated HNO_3 (61%, UN-2031, Kanto, Japan; or 65–68%, CAS:7697–37-2, Jing Rui, China) at up to 120 °C. HNO_3 without plant samples was used as a blank control. The concentrations of elements in the digested solution were determined using inductively coupled plasma MS (ICP-MS 7700X, Agilent Technologies, CA, USA; or NexION 1000G, PerkinElmer, USA), as described previously [53].

Statistical analysis

Statistical tests were performed using Tukey's test. The significance of differences was defined as $P < 0.05$.

Supplementary Information

The online version contains supplementary material available at https://doi.org/10.1186/s13059-026-04046-6.

Additional file 1: Supplementary Figures. Fig. S1. Sample preparation and cell type property in snRNA-Seq of node I. Fig. S2. UMAP and tSNE visualization of 11 cell clusters in rice node I. Fig. S3. Expression patterns of selected top enriched genes for 11 cell types. Fig. S4. Expression patterns of marker or enriched genes in each cell type. Fig. S5. Tissue-specific expression of *OsMT2c* in node I. Fig. S6. Spatial ionomics and expression patterns of candidate genes. Fig. S7. Rb and Sb concentration in the short-term labeling experiment. Fig. S8. Expression of the MTP family in rice node I. Fig. S9. Phylogenetic tree and multiple alignment of OsMTP7. Fig. S10. Tissue localization of OsMTP9 in node I. Fig. S11. Expression profile of *OsMTP7*. Fig. S12. Subcellular localization of OsMTP7. Fig. S13. Effect of *OsMTP7* knockout on plant growth at the reproductive stage. Fig. S14. Effect of *OsMTP7* knockout on ions concentrations in straw and brown rice. Fig. S15. Effect of *OsMTP7* knockout on the accumulation and uptake of ions at the vegetative stage. Fig. S16. Expression of genes involved in Mn homeostasis in roots. Fig. S17. Spikelet phenotype and Venn diagrams of bulk RNA-seq. Fig. S18. Subcellular localization of OsMTP7 in yeast. Fig. S19. Transport assay of OsMTP7 for Cu, Fe and Zn in yeast. Fig. S20. Expression pattern of *OsNRAMP3* in node I.

Additional file 2: Supplementary Tables. Table S1. Overview of snRNA-seq data. Table S2. Cluster-enriched genes information. Table S3. Expression pattern of transporter genes. Table S4. Bulk RNA-seq of spikelets. Table S5. Primers used in this study.

Acknowledgements
We thank Dr. Jing Che (Institute of Soil Science, Chinese Academy of Sciences, Nanjing, China) for the discussion and suggestion. We thank the Yunnan Revitalization Talent Support Program-Young Talents Project.

Peer review information
Jixian Zhai and Wenjing She were the primary editors of this article and managed its editorial process and peer review in collaboration with the rest of the editorial team. The peer-review history is available in the online version of this article.

Authors' contributions
G.J.L. conceived and designed the experiments. H.L., H.J., M.N., F.D., W.C., O.Y., J.C., X.L., L.S., S.Z., N.Y., F.H., J.F.M., and G.J.L. performed the experiments and took part in data analysis and discussion. N.Y., and J.F.M. provided critical suggestion to the experiments. G.J.L. wrote the manuscript. All authors read and approved the final manuscript.

Funding
This work was supported by grants from the National Natural Science Foundation of China (32260450 and 32372055 to G.J.L.; 32370285 to F.D.), the Yunnan Fundamental Research Projects (202301BF070001-018, 202201AW070003 and 202201AU070013 to G.J.L.), the Japan Society for the Promotion of Science (JSPS; KAKENHI grant no. 21H05034 to J.F.M.), the National Key Research and Development Program of China (2023YFD23020001 to F.H.), New Cornerstone Science Foundation (NIC202341 to F.H.), the Hubei Hongshan Laboratory (2021hskf004 to F.D.), and Yunnan University and Yunnan Education Department (KC-252513720 to H.L.).

Data availability
The datasets generated and analyzed during the current study are available in the following repositories: The raw single-nucleus RNA-seq (snRNA-seq) data have been deposited in the NCBI Sequence Read Archive (SRA) under BioProject PRJNA1331938 [100], and the processed gene expression matrix has been deposited in the NCBI Gene Expression Omnibus (GEO) under accession GSE308757 [101]. The analysis code used in this study is publicly available at GitHub: https://github.com/JHL0410/scRNA-seq-code [102]. The source code is released under the GNU General Public License v3.0 (GPL-3.0) and has been archived in Zenodo [103]. Our reference dataset for the correlation analysis is available at http://ibi.zju.edu.cn/plantscrnadb/#/ [49]. The version of the code used for this manuscript is available at: https://doi.org/10.5281/zenodo.18954644 [103]. All microscopy data used for quantification on Figshare [104]. The raw bulk RNA-seq data have been deposited in the Genome Sequence Archive (GSA) under accession number CRA030039 [105, 106].

Declarations

Ethics approval and consent to participate
Not applicable.

Consent for publication
Not applicable.

Competing interests
The authors declare no competing interests.

Received: 22 May 2025 Accepted: 17 March 2026
Published online: 27 March 2026

References

1. Marschner P, editor. Marschner's Mineral Nutrition of Higher Plants. 3rd ed. Amsterdam: Academic Press; 2012.
2. Yamaji N, Ma JF. The node, a hub for mineral nutrient distribution in graminaceous plants. Trends Plant Sci. 2014;19:556–63.
3. Yamaji N, Ma JF. Node-controlled allocation of mineral elements in Poaceae. Curr Opin Plant Biol. 2017;39:18–24.
4. Ding G, Lei GJ, Yamaji N, Yokosho K, Mitani-Ueno N, Huang S, et al. Vascular cambium-localized AtSPDT mediates xylem-to-phloem transfer of phosphorus for its preferential distribution in Arabidopsis. Mol Plant. 2020;13:99–111.
5. Huang S, Wang P, Yamaji N, Ma JF. Plant nutrition for human nutrition: hints from rice research and future perspectives. Mol Plant. 2020;13:825–35.
6. Gu M, Huang H, Hisano H, Ding G, Huang S, Mitani-Ueno N, et al. A crucial role for a node-localized transporter, HvSPDT, in loading phosphorus into barley grains. New Phytol. 2022;234:1249–61.
7. Hu Y, Zhang M, Wang K, Tan P, Jing S, Han W, et al. ZmNPF7.10 confers potassium and nitrogen distribution from node to leaf in maize. New Phytol. 2025;245:2698–714.
8. Hoshikawa K. The growing rice plant. An anatomical monograph. Nosan Gyoson Bunka. 1989:199–205.
9. Yamaji N, Sakurai G, Mitani-Ueno N, Ma JF. Orchestration of three transporters and distinct vascular structures in node for intervascular transfer of silicon in rice. Proc Natl Acad Sci U S A. 2015;112:11401–6.
10. Sasaki A, Yamaji N, Mitani-Ueno N, Kashino M, Ma JF. A node-localized transporter OsZIP3 is responsible for the preferential distribution of Zn to developing tissues in rice. Plant J. 2015;84:374–84.
11. Yamaji N, Yoshioka Y, Huang S, Miyaji T, Sasaki A, Ma JF. An oligo peptide transporter family member, OsOPT7, mediates xylem unloading of Fe for its preferential distribution in rice. New Phytol. 2024;242:2620–34.
12. Che J, Yamaji N, Miyaji T, Mitani-Ueno N, Kato Y, Shen RF, et al. Node-localized transporters of phosphorus essential for seed development in rice. Plant Cell Physiol. 2020;61:1387–98.
13. Deng F, Yamaji N, Xia J, Ma JF. A member of the heavy metal P-type ATPase OsHMA5 is involved in xylem loading of copper in rice. Plant Physiol. 2013;163:1353–62.
14. Che J, Yokosho K, Yamaji N, Ma JF. A vacuolar phytosiderophore transporter alters iron and zinc accumulation in polished rice grains. Plant Physiol. 2019;181:276–88.
15. Shao JF, Yamaji N, Huang S, Ma JF. Fine regulation system for distribution of boron to different tissues in rice. New Phytol. 2021;230:656–68.
16. Kobayashi NI, Yamaji N, Yamamoto H, Okubo K, Ueno H, Costa A, et al. OsHKT1;5 mediates Na^+ exclusion in the vasculature to protect leaf blades and reproductive tissues from salt toxicity in rice. Plant J. 2017;91:657–70.
17. Yamaji N, Xia JX, Mitani-Ueno N, Yokosho K, Ma JF. Preferential delivery of zinc to developing tissues in rice is mediated by P-type heavy metal ATPase OsHMA2. Plant Physiol. 2013;162:927–39.
18. Mu S, Yamaji N, Sasaki A, Luo L, Du B, Che J, et al. A transporter for delivering zinc to the developing tiller bud and panicle in rice. Plant J. 2021;105:786–99.
19. Shao JF, Yamaji N, Shen RF, Ma JF. The key to Mn homeostasis in plants: regulation of Mn transporters. Trends Plant Sci. 2017;22:215–24.
20. Lilay GH, Thiébaut N, du Mee D, Assunção AGL, Schjoerring JK, Husted S, et al. Linking the key physiological functions of essential micronutrients to their deficiency symptoms in plants. New Phytol. 2024;242:881–902.
21. Sasaki A, Yamaji N, Yokosho K, Ma JF. Nramp5 is a major transporter responsible for manganese and cadmium uptake in rice. Plant Cell. 2012;24:2155–67.
22. Ueno D, Sasaki A, Yamaji N, Miyaji T, Fujii Y, Takemoto Y, et al. A polarly localized transporter for efficient manganese uptake in rice. Nat Plants. 2015;1:15170.
23. Chang JD, Huang S, Yamaji N, Zhang W, Ma JF, Zhao FJ. OsNRAMP1 transporter contributes to cadmium and manganese uptake in rice. Plant Cell Environ. 2020;43:2476–91.
24. Chen ZH, Fujii Y, Yamaji N, Masuda S, Takemoto Y, Kamiya T, et al. Mn tolerance in rice is mediated by MTP8.1, a member of the cation diffusion facilitator family. J Exp Bot. 2013;64:4375–87.
25. Takemoto Y, Tsunemitsu Y, Fujii-Kashino M, Mitani-Ueno N, Yamaji N, Ma JF, et al. The tonoplast-localized transporter MTP8.2 contributes to manganese detoxification in the shoots and roots of *Oryza sativa* L. Plant Cell Physiol. 2017;58:1573–82.
26 Farthing EC, Menguer PK, Fett JP, Williams LE. OsMTP11 is localised at the Golgi and contributes to Mn tolerance. Sci Rep. 2017;7:15258.
27. Xu E, Wu M, Liu Y, Tai Y, Zha W, Gong C, et al. The Golgi-localized transporter OsPML3 is involved in manganese homeostasis and complex N-glycan synthesis in rice. J Exp Bot. 2023;74:1853–72.
28. Ishimaru Y, Masuda H, Bashir K, Inoue H, Tsukamoto T, Takahashi M, et al. Rice metal-nicotianamine transporter, OsYSL2, is required for the long-distance transport of iron and manganese. Plant J. 2010;62:379–90.
29. Sasaki A, Yamaji N, Xia JX, Ma JF. OsYSL6 is involved in the detoxification of excess manganese in rice. Plant Physiol. 2011;157:1832–40.
30. Yamaji N, Sasaki A, Xia JX, Yokosho K, Ma JF. A node-based switch for preferential distribution of manganese in rice. Nat Commun. 2013;4:2442.
31. Huang S, Konishi N, Yamaji N, Ma JF. Local distribution of manganese to leaf sheath is mediated by OsNramp5 in rice. New Phytol. 2023;241:1708–19.
32 Yu X, Liu Z, Sun X. Single-cell and spatial multi-omics in the plant sciences: Technical advances, applications, and perspectives. Plant Commun. 2023;4:100508.
33 Zheng D, Xu J, Lu Y, Chen H, Chu Q, Fan L. Recent progresses in plant single-cell transcriptomics. Crop Design. 2023;2:100041.
34. Farmer A, Thibivilliers S, Ryu KH, Schiefelbein J, Libault M. Single-nucleus RNA and ATAC sequencing reveals the impact of chromatin accessibility on gene expression in Arabidopsis roots at the single-cell level. Mol Plant. 2021;14:372–83.
35. Wang Y, Huan Q, Li K, Qian W. Single-cell transcriptome atlas of the leaf and root of rice seedlings. J Genet Genom. 2021;48:881–98.

36. Zong J, Wang L, Zhu L, Bian L, Zhang B, Chen X, et al. A rice single cell transcriptomic atlas defines the developmental trajectories of rice floret and inflorescence meristems. New Phytol. 2022;234:494–512.
37. Swift J, Luginbuehl LH, Hua L, Schreier TB, Donald RM, Stanley S, et al. Exaptation of ancestral cell-identity networks enables C4 photosynthesis. Nature. 2024;636:143–50.
38. Zhu M, Zhang M, Huang K, Lu F, Wang H, Zhao S, et al. Single-cell transcriptome sequencing reveals the mechanism regulating rice plumule development. Crop J. 2024;12:688–97.
39. Wang X, Huang H, Jiang S, Kang J, Li D, Wang K, et al. A single-cell multi-omics atlas of rice. Nature. 2025;644:722–30.
40. Shang L, He W, Wang T, Yang Y, Xu Q, Zhao X, et al. A complete assembly of the rice Nipponbare reference genome. Mol Plant. 2023;16:1232–6.
41. Kudo T, Kawai A, Yamaya T, Hayakawa T. Cellular distribution of ACT domain repeat protein 9, a nuclear localizing protein, in rice (*Oryza sativa*). Physiol Plant. 2008;133:167–79.
42. Fang L, Zhao F, Cong Y, Sang X, Du Q, Wang D, et al. Rolling-leaf14 is a 2OG-Fe (II) oxygenase family protein that modulates rice leaf rolling by affecting secondary cell wall formation in leaves. Plant Biotechnol J. 2012;10:524–32.
43. Li Y, Ouyang J, Wang YY, Hu R, Xia K, Duan J, et al. Disruption of the rice nitrate transporter OsNPF2.2 hinders root-to-shoot nitrate transport and vascular development. Sci Rep. 2015;5:9635.
44. Lei GJ, Yamaji N, Ma JF. Two metallothionein genes highly expressed in rice nodes are involved in distribution of Zn to the grain. New Phytol. 2021;229:1007–20.
45. Bang SW, Lee DK, Jung H, Chung PJ, Kim YS, Choi YD, et al. Overexpression of OsTF1L, a rice HD-Zip transcription factor, promotes lignin biosynthesis and stomatal closure that improves drought tolerance. Plant Biotechnol J. 2018;17:118–31.
46. Kumar V, Kim SH, Adnan MR, Heo J, Jeong JH, Priatama RA, et al. Tiller outgrowth in rice (*Oryza sativa* L.) is controlled by OsGT1, which acts downstream of FC1 in a PhyB-independent manner. J Plant Biol. 2021;64:417–30.
47. Liu X, Li M, Liu K, Tang D, Sun M, Li Y, et al. Semi-rolled leaf2 modulates rice leaf rolling by regulating abaxial side cell differentiation. J Exp Bot. 2016;67:2139–50.
48. Sun W, Gao D, Xiong Y, Tang X, Xiao X, Wang C, et al. Hairy leaf 6, an AP2/ERF transcription factor, interacts with OsWOX3B and regulates trichome formation in rice. Mol Plant. 2017;10:1417–33.
49. Zheng D, Lu X, Lu Y, Liang P, Shang N, Xu J, et al. PlantscRNAdb 4.0: improved marker identification and annotation under a cell type uniformity for plants. Mol Plant. 2025;19(3):673-688.
50. Hirano K, Aya K, Kondo M, Okuno A, Morinaka Y, Matsuoka M. OsCAD2 is the major CAD gene responsible for monolignol biosynthesis in rice culm. Plant Cell Rep. 2011;31:91–101.
51. Chai M, Bellizzi M, Wan C, Cui Z, Li Y, Wang G-L. The NAC transcription factor OsSWN1 regulates secondary cell wall development in *Oryza sativa*. J Plant Biol. 2015;58:44–51.
52. Che J, Yamaji N, Ma JF. Role of a vacuolar iron transporter OsVIT2 in the distribution of iron to rice grains. New Phytol. 2021;230:1049–62.
53. Ning M, Liu SJ, Deng F, Huang L, Li H, Che J, et al. A vacuolar transporter plays important roles in zinc and cadmium accumulation in rice grain. New Phytol. 2023;239:1919–34.
54. Ueno D, Yamaji N, Kono I, Huang CF, Ando T, Yano M, et al. Gene limiting cadmium accumulation in rice. Proc Natl Acad Sci U S A. 2010;107:16500–5.
55. Song WY, Yamaki T, Yamaji N, Ko D, Jung KH, Fujii-Kashino M, et al. A rice ABC transporter, OsABCC1, reduces arsenic accumulation in the grain. Proc Natl Acad Sci U S A. 2014;111:15699–704.
56. Huang XY, Deng F, Yamaji N, Pinson SR, Fujii-Kashino M, Danku J, et al. A heavy metal P-type ATPase OsHMA4 prevents copper accumulation in rice grain. Nat Commun. 2016;7:12138.
57. Guo R, Zhang Q, Ying Y, Liao W, Liu Y, Whelan J, et al. Functional characterization of the three *Oryza sativa* SPX-MFS proteins in maintaining phosphate homoeostasis. Plant Cell Environ. 2022;46:1264–77.
58. Stanton C, Sanders D, Kramer U, Podar D. Zinc in plants: integrating homeostasis and biofortification. Mol Plant. 2022;15:65–85.
59. Pumplin N, Harrison MJ. Live-cell imaging reveals periarbuscular membrane domains and organelle location in *Medicago truncatula* roots during arbuscular mycorrhizal symbiosis. Plant Physiol. 2009;151:809–19.
60. Sauter M, Lorbiecke R, OuYang B, Pochapsky TC, Rzewuski G. The immediate-early ethylene response gene OsARD1 encodes an acireductone dioxygenase involved in recycling of the ethylene precursor S-adenosylmethionine. Plant J. 2005;44:718–29.
61. Mei C, Qi M, Sheng G, Yang Y. Inducible overexpression of a rice allene oxide synthase gene increases the endogenous jasmonic acid level, PR gene expression, and host resistance to fungal infection. Mol Plant-Microbe Interact®. 2006;19:1127–37.
62. Xu M, Ross Wilderman P, Morrone D, Xu J, Roy A, Margis-Pinheiro M, et al. Functional characterization of the rice kaurene synthase-like gene family. Phytochemistry. 2007;68:312–26.
63. Wang E, Wang J, Zhu X, Hao W, Wang L, Li Q, et al. Control of rice grain-filling and yield by a gene with a potential signature of domestication. Nat Genet. 2008;40:1370–4.
64. Song WY, Lee HS, Jin SR, Ko D, Martinoia E, Lee Y, et al. Rice PCR1 influences grain weight and Zn accumulation in grains. Plant Cell Environ. 2015;38:2327–39.
65. Burman N, Bhatnagar A, Khurana JP. OsbZIP48, a HY5 transcription factor ortholog, exerts pleiotropic effects in light-regulated development. Plant Physiol. 2018;176:1262–85.
66. Tao J, Liang W, An G, Zhang D. OsMADS6 controls flower development by activating rice FACTOR OF DNA METHYLATION LIKE1. Plant Physiol. 2018;177:713–27.
67. Wang L, Ming L, Liao K, Xia C, Sun S, Chang Y, et al. Bract suppression regulated by the miR156/529-SPLs-NL1-PLA1 module is required for the transition from vegetative to reproductive branching in rice. Mol Plant. 2021;14:1168–84.
68. Zhang L, He G, Li Y, Yang Z, Liu T, Xie X, et al. PIL transcription factors directly interact with SPLs and repress tillering/branching in plants. New Phytol. 2021;233:1414–25.

69. Sun Y, Wang B, Ren J, Zhou Y, Han Y, Niu S, et al. OsbZIP18, a positive regulator of serotonin biosynthesis, negatively controls the UV-B tolerance in rice. Int J Mol Sci. 2022;23:3215.
70. Wang Z, Zhang B, Chen Z, Wu M, Chao D, Wei Q, et al. Three OsMYB36 members redundantly regulate Casparian strip formation at the root endodermis. Plant Cell. 2022;34:2948–68.
71. Wang H, Tong X, Tang L, Wang Y, Zhao J, Li Z, et al. RLB (RICE LATERAL BRANCH) recruits PRC2-mediated H3K27 tri-methylation on OsCKX4 to regulate lateral branching. Plant Physiol. 2022;188:460–76.
72. Alscher RG, Erturk N, Heath LS. Role of superoxide dismutases (SODs) in controlling oxidative stress in plants. J Exp Bot. 2002;53:1331–41.
73. Hu L, Liang W, Yin C, Cui X, Zong J, Wang X, et al. Rice MADS3 regulates ROS homeostasis during late anther development. Plant Cell. 2011;23:515–33.
74. Sun L, Wei YQ, Wu KH, Yan JY, Xu JN, Wu YR, et al. Restriction of iron loading into developing seeds by a YABBY transcription factor safeguards successful reproduction in Arabidopsis. Mol Plant. 2021;14:1624–39.
75. Huang CF, Yamaji N, Chen Z, Ma JF. A tonoplast-localized half-size ABC transporter is required for internal detoxification of aluminum in rice. Plant J. 2012;69:857–67.
76. Jüschke C, Wächter A, Schwappach B, Seedorf M. SEC18/NSF-independent, protein-sorting pathway from the yeast cortical ER to the plasma membrane. J Cell Biol. 2005;169:613–22.
77. Yamaji N, Takemoto Y, Miyaji T, Mitani-Ueno N, Yoshida KT, Ma JF. Reducing phosphorus accumulation in rice grains with an impaired transporter in the node. Nature. 2017;541:92–5.
78. Moore KL, Chen Y, van de Meene AML, Hughes L, Liu W, Geraki T, et al. Combined NanoSIMS and synchrotron X-ray fluorescence reveal distinct cellular and subcellular distribution patterns of trace elements in rice tissues. New Phytol. 2013;201:104–15.
79. Yamaji N, Ma JF. Bioimaging of multiple elements by high-resolution LA-ICP-MS reveals altered distribution of mineral elements in the nodes of rice mutants. Plant J. 2019;99:1254–63.
80. Delhaize E, Gruber BD, Pittman JK, White RG, Leung H, Miao YS, et al. A role for the *AtMTP11* gene of Arabidopsis in manganese transport and tolerance. Plant J. 2007;51:198–210.
81. Tanaka N, Fujiwara T, Tomioka R, Kramer U, Kawachi M, Maeshima M. Characterization of the histidine-rich loop of Arabidopsis vacuolar membrane zinc transporter AtMTP1 as a sensor of zinc level in the cytosol. Plant Cell Physiol. 2015;56:510–9.
82. Chu HH, Car S, Socha AL, Hindt MN, Punshon T, Guerinot ML. The Arabidopsis MTP8 transporter determines the localization of manganese and iron in seeds. Sci Rep. 2017;7:11024.
83. Zheng L, Yamaji N, Yokosho K, Ma JF. YSL16 is a phloem-localized transporter of the copper-nicotianamine complex that is responsible for copper distribution in rice. Plant Cell. 2012;24:3767–82.
84. Gao H, Xie W, Yang C, Xu J, Li J, Wang H, et al. NRAMP2, a trans-Golgi network-localized manganese transporter, is required for Arabidopsis root growth under manganese deficiency. New Phytol. 2017;217:179–93.
85. Yang CH, Wang C, Singh S, Fan N, Liu S, Zhao L, et al. Golgi-localised manganese transporter PML3 regulates *Arabidopsis* growth through modulating Golgi glycosylation and cell wall biosynthesis. New Phytol. 2021;231:2200–14.
86. He J, Yang B, Hause G, Rössner N, Peiter-Volk T, Schattat MH, et al. The trans-Golgi-localized protein BICAT3 regulates manganese allocation and matrix polysaccharide biosynthesis. Plant Physiol. 2022;190:2579–600.
87. Ma JF, Tamai K, Ichii M, Wu GF. A rice mutant defective in Si uptake. Plant Physiol. 2002;130:2111–7.
88. Slyper M, Porter CBM, Ashenberg O, Waldman J, Drokhlyansky E, Wakiro I, et al. A single-cell and single-nucleus RNA-Seq toolbox for fresh and frozen human tumors. Nat Med. 2020;26:792–802.
89. Galbraith D, Loureiro J, Antoniadi I, Bainard J, Bureš P, Cápal P, et al. Best practices in plant cytometry. Cytometry A. 2021;99:311–7.
90. Galbraith DW, Sun G. Flow cytometry and sorting in Arabidopsis. Arabidopsis Protocols. 2021:255–294.
91. Dobin A, Davis CA, Schlesinger F, Drenkow J, Zaleski C, Jha S, et al. STAR: ultrafast universal RNA-seq aligner. Bioinformatics. 2013;29:15–21.
92. Van der Maaten L, Hinton G. Visualizing data using t-SNE. J Mach Learn Res. 2008;9:2579.
93. Becht E, McInnes L, Healy J, Dutertre CA, Kwok IW, Ng LG, et al. Dimensionality reduction for visualizing single-cell data using UMAP. Nat Biotechnol. 2019;37:38–44.
94. Yu H, Xu Y, Tan EL, Kumar PP. AGAMOUS-LIKE 24, a dosage-dependent mediator of the flowering signals. Proc Natl Acad Sci U S A. 2002;99:16336–41.
95. Fuse T, Sasaki T, Yano M. Ti-plasmid vectors useful for functional analysis of rice genes. Plant Biotechnol J. 2001;18:219–22.
96. Hiei Y, Ishida Y, Kasaoka K, Komari T. Improved frequency of transformation in rice and maize by treatment of immature embryos with centrifugation and heat prior to infection with *Agrobacterium tumefaciens*. Plant Cell Tissue Organ Cult. 2006;87:233–43.
97. Tamai K, Ma JF. Reexamination of silicon effects on rice growth and production under field conditions using a low silicon mutant. Plant Soil. 2008;307(1–2):21–7.
98. Chen S, Tao L, Zeng L, Vega-Sanchez ME, Umemura K, Wang GL. A highly efficient transient protoplast system for analyzing defence gene expression and protein–protein interactions in rice. Mol Plant Pathol. 2006;7:417–27.
99. Mikami M, Toki S, Endo M. Comparison of CRISPR/Cas9 expression constructs for efficient targeted mutagenesis in rice. Plant Mol Biol. 2015;88:561–72.
100. Li H, Jin H, Ning M, Deng F, Cheng J, Chen W, et al. Rice High-throughput single-nucleus RNA sequencing. Datasets. Datasets sequence read archive. 2025. https://www.ncbi.nlm.nih.gov/sra/?term=PRJNA1331938.
101. Li H, Jin H, Ning M, Deng F, Cheng J, Chen W, et al. Single-cell transcriptome profiling of Oryza sativa node I at booting, flowering, and grain filling stages. Datasets. Gene Expression Omnibus. 2025. https://www.ncbi.nlm.nih.gov/geo/query/acc.cgi?acc=GSE308757.
102. Li H, Jin H, Ning M, Deng F, Cheng J, Chen W, et al. scRNA-seq-code. Github. 2026. https://github.com/JHL0410/scRNA-seq-code.
103. Li H, Jin H, Ning M, Deng F, Cheng J, Chen W, et al. JHL0410/scRNA-seq-code: analysis code. Zenodo. 2026. https://doi.org/10.5281/zenodo.18954643.

104. Li H, Jin H, Ning M, Deng F, Cheng J, Chen W, et al. osmtp7 pollen viability determination. pollen staining by 1% KI–I Figshare. 2026. https://doi.org/10.6084/m9.figshare.31671853.
105. Li H, Jin H, Ning M, Deng F, Cheng J, Chen W, et al. Transcriptomic analysis of *osmtp7* rice mutant spikelets reveals disruptions in redox homeostasis, hormone metabolism, and cell wall processes leading to male sterility. Datasets. Datasets genome sequence archive. 2025. https://ngdc.cncb.ac.cn/gsa/browse/CRA030039.
106. Zhang S, Chen X, Jin E, Wang A, Chen T, Zhang X, et al. The GSA family in 2025: a broadened sharing platform for multi-omics and multimodal data. bioRxiv. 2025:2025.2003. 2031.646270.

Publisher's Note